Blume-Emery-Griffiths-Potts model in two dimensions: Phase diagram and critical properties from a position-space renormalization group*

A. N. Berker and Michael Wortis
Physics Department and Materials Research Laboratory, University of Illinois at Urbana-Champaign, Urbana, Illinois 61801
(Received 14 June 1976)

The spin-1 Ising model on the square lattice with nearest-neighbor ferromagnetic exchange interactions [both bilinear (J) and biquadratic (K)] and crystal-field interaction (Δ) is studied via a renormalization-group transformation in position space. The phase diagram in J, K, Δ space is found to have one surface of critical phase transitions and two surfaces of first-order phase transitions. These surfaces are variously bounded by an ordinary tricritical line, an isolated critical line, and a line of critical end points. These three lines join at a special tricritical point corresponding to the transition of the three-state Potts model. The over-all phase diagram is qualitatively similar to that obtained with the mean-field approximation, except in the vicinity of the Potts transition where a four-phase coexistence line in mean-field theory shrinks into a special tricritical point in renormalization-group theory. Symmetry considerations guide the construction of our truncated renormalization-group transformation. The global connectivity and local exponents of the thirteen separate fixed points underlying this quite complicated structure are determined. Local analysis with respect to magnetic field (H) and another odd interaction (L) is performed. A one-adjusted-parameter version of our transformation yields remarkably quantitative results, predicting the Potts transition temperature, for example, within 0.3% of the exact value.

I. INTRODUCTION: POSITION-SPACE RENORMALIZATION-GROUP METHOD AND THE BLUME-EMERY-GRIFFITHS MODEL

The direct application of Wilson's renormalization-group approach[1] to phase transitions[2] in lattice systems, using a rescaling[3] transformation in position space, has lately received considerable attention.[4-24] Such transformations are constructed by associating one collective spin with each group of neighboring initial spins in the lattice, and then by summing in the position-space representation of the partition function over all degrees of freedom orthogonal to the collective spins. In this process, one usually[4] resorts to some truncating[25] approximation to control the arbitrary interactions otherwise generated. Niemeijer and van Leeuwen,[5] Kadanoff and coworkers,[6,7] and others[8-14] solidly established this method through the study of the critical phase transition in the two-dimensional spin-$\frac{1}{2}$ Ising model, where Onsager's exact solution[26] is available for comparison.

These very impressive results have spurred applications to more complex problems about which there is little exact information, such as phase transitions in systems with higher lattice dimensionality,[7,15] more complicated spin kinematics,[16-19] or random bonds.[20] Most work on these lines has focused on a single nontrivial fixed point and concentrated on calculating critical exponents and critical interactions. By contrast, in the research reported here we use the position-space renormalization-group (PSRG) method to study a model with a very rich phase diagram, exhibiting a wide variety of transitions of first and higher order. We find a total of 13 different fixed points, yielding first-order phase boundaries, critical and (ordinary and special) tricritical points, and critical end points. All of these arise from a single, very simple set of recursion relations. The *global* phase diagram is determined by the topology of the PSRG flows linking the various fixed points.[27] Local analysis of the recursion relations near the fixed points gives all the exponents, with a precision which appears remarkably good in those cases where comparison with other data is possible.

We study the Blume-Emery-Griffiths (BEG) model[28] on the square lattice ($d=2$). This is just a spin-1 Ising model with the Hamiltonian

$$\mathcal{H}(J,K,\Delta;\{s\}) = J\sum_{\langle ij\rangle} s_i s_j + K\sum_{\langle ij\rangle} s_i^2 s_j^2 - \Delta\sum_i s_i^2, \quad s_i = 0, \pm 1, \tag{1.1}$$

where $\langle ij\rangle$ indicates summation over nearest-neighbor pairs (we restrict this study to $J, K \geq 0$). The usual $-1/k_BT$ factor has been absorbed into this Hamiltonian. The terms on the right-hand side are, respectively, the bilinear exchange, biquadratic exchange, and crystal-field interactions. In order to obtain a complete description of the phase transitions, vanishingly small magnetic-field-like (odd) perturbations

$$H\sum_i s_i + L\sum_{\langle ij\rangle}(s_i s_j^2 + s_i^2 s_j) \tag{1.2}$$

must also be considered.

Blume, Emergy, and Griffiths[28] introduced this model to describe phase separation and superfluid ordering in He^3-He^4 mixtures. The BEG model was subsequently reinterpreted to describe phase transitions in simple[29] and multicomponent[29-31] fluids. References 28–31 used the mean-field approximation (MFA). The BEG model on the ($d=3$) fcc lattice was studied by series[32] and Monte Carlo[33] methods. Two other works treated the square lattice: Arora and Landau[34] performed a Monte Carlo calculation. Burkhardt[23] has recently obtained local ordinary tricritical properties by a PSRG transformation[7] different from ours. He has not obtained the unified global phase diagram and other local features presented here.

The plan of our presentation is as follows: Sec. II collects several items of exact information on the phase diagram of the BEG model which follow from simple, general considerations. We then exhibit (for later comparison with PSRG results) the MFA phase diagram (Figs. 2, 3). Section III develops our PSRG transformation. Symmetry considerations, based on the exact information of Sec. II, guide this process. We use two versions of our transformation: one with no free parameters, the other with a single parameter which is adjusted to fit the known[26] critical temperature of the spin-$\frac{1}{2}$ Ising model. Section III can be skipped by readers uninterested in renormalization-group technology. Our results are summarized by Figs. 7 and 8 (phase diagram) and Tables III–VII (exponents). Most of these results are discussed in Sec. IV. The J, K, Δ phase diagram is composed of three surfaces: two of first-order transitions and one of critical (second order) transitions. These three surfaces meet, with no intervening higher-order transition, along a semiinfinite line of critical end points, which terminates at a special tricritical (Potts) point. Two other lines terminate at this Potts point: One is a locus of ordinary tricritical points, which separates the critical surface and one of the first-order surfaces. The other is an isolated line of critical points bounding the remaining first-order surface. We locate the 13 separate fixed points underlying this quite complicated structure and study the connectivity of the renormalization-group flows linking them. Finally in Sec. V we consider the three-state Potts model,[36,37] to which the BEG model reduces for specific values of the interaction constant ratios. Our PSRG phase diagram is qualitatively similar to the MFA phase diagram except in the vicinity of this Potts transition, where a four-phase coexistence line in mean-field theory shrinks into a special tricritical point in renormalization-group theory, in agreement with previous Potts model treatments.[38,39] The one-adjusted-parameter version of our transformation yields remarkably quantitative results: for example, it gives a Potts transition temperature within 0.3% of the exact value.[36]

II. EXACT INFORMATION AND THE MEAN-FIELD PHASE DIAGRAM

The BEG model defined by the Hamiltonian (1.1) has two order parameters,[28-31] namely the magnetization M and the quadrupole order parameter Q:

$$M(J,K,\Delta) \equiv \langle s_i \rangle = Z^{-1} \sum_{\{s\}} s_i e^{\mathcal{H}} , \tag{2.1a}$$

$$Q(J,K,\Delta) \equiv \langle s_i^2 \rangle = Z^{-1} \sum_{\{s\}} s_i^2 e^{\mathcal{H}} , \tag{2.1b}$$

where the sums are over all spin configurations, the translational invariance of (1.1) makes i arbitrary, and Z is the partition function:

$$Z(J,K,\Delta) = \sum_{\{s\}} e^{\mathcal{H}} . \tag{2.1c}$$

We restrict this study to $J, K \geq 0$, so that no sublattice order parameter must be introduced. We begin by extracting from simple, general considerations several items of exact information, which in Sec. III will guide the construction of our PSRG transformation. We shall accumulate these in Fig. 1. Then, the MFA phase diagram will be recalled (Figs. 2 and 3).

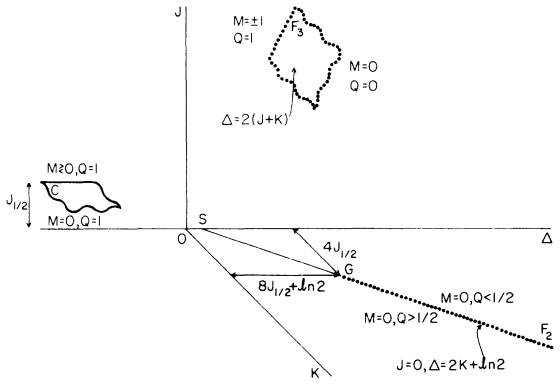

FIG. 1. Some exact information on the BEG phase diagram. C and F_3 are planar segments of critical and first-order transition surfaces respectively. G is the Griffiths-Onsager critical point, and GF_2 is a first-order transition line. The relationship between the locations of C and G is exhibited. These features are obtained in Secs. II A–II C from simple, general considerations. They guide the construction of our renormalization-group transformation in Sec. III.

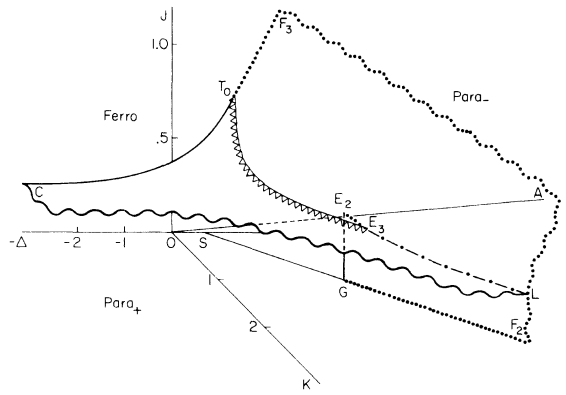

FIG. 2. BEG phase diagram obtained with the mean-field approximation, discussed in Sec. II D. Critical and first-order transitions are respectively drawn with dark full and dotted lines. Wavy lines denote smooth continuation of surfaces. The two coexisting ferromagnetic phases (Ferro) and each of the two paramagnetic phases (Para$_\pm$) are separated by the critical surface CT_0E_3L, and by the first-order surfaces $F_3T_0E_3L$ (three-phase coexistence) and F_2GE_2L (two-phase coexistence). T_0E_3 is an ordinary tricritical line (triangles), GE_2 is an isolated critical line, and E_3L is a critical end line (dash-dotted). E_2 and E_3, respectively, are critical and tricritical end points; between, E_2E_3 is a four-phase coexistence line. Features along the Potts axis $0A$ are discussed in Sec. V B. Representative constant-K cross sections of this MFA phase diagram are in Fig. 3.

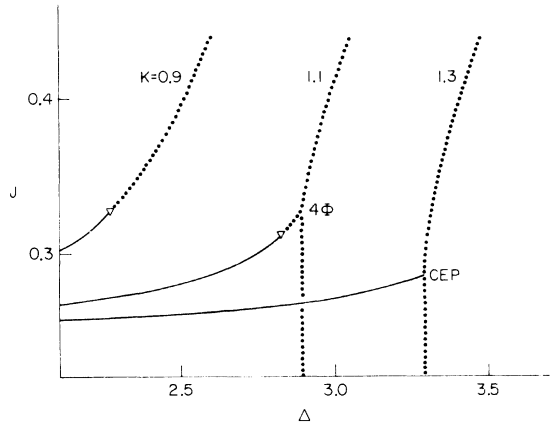

FIG. 3. Representative constant-K cross sections of the BEG phase diagram (Fig. 2) obtained with the mean-field approximation. Critical and first-order transitions are, respectively, drawn with full and dotted lines. The ordinary tricritical points (triangles), the four-phase coexistence point (4Φ), and the critical end point (CEP) are indicated. The critical and first-order lines meeting at the tricritical point have equal slopes. The three first-order lines at the four-phase coexistence point have different slopes (one has infinite slope). Both first-order lines at the critical end point have infinite slope, while the critical line has finite slope.

A. Regions $|\Delta| \gg 1$

At $\Delta \ll -1$, the configurations $\{s_i = \pm 1\}$ in which all spins are nonzero completely dominate the ensemble averages in (2.1). When we restrict the sums to these configurations, the second and third terms in (1.1) become just additive constants which do not affect further ordering, and the Hamiltonian reduces to

$$\mathcal{H}(J;\{s\}) = J \sum_{\langle ij \rangle} s_i s_j , \quad s_i = \pm 1 , \tag{2.2}$$

which describes the two-dimensional spin-$\frac{1}{2}$ Ising model, exactly solved by Onsager.[26] Accordingly, we expect a critical[40] (second-order) phase transition at $J = J_{1/2}$. Thus, the $\Delta \ll -1$ and $K \geq 0$ region has a segment of critical surface parallel to the $J = 0$ plane at a height $J_{1/2}$ above it. This segment is labelled C in Fig. 1. Above it, two low-temperature ferromagnetic phases coexist with $M \gtrless 0$, $Q = 1$ (the inverse interaction measures the temperature); below it, there is a paramagnetic phase with $M = 0$, $Q = 1$.

At $\Delta \gg 1$ and J, K finite, the configuration $\{s_i = 0\}$ in which all spins are zero completely dominates the ensemble. Therefore both M and Q vanish.

B. Asymptotic first-order transition

In the $2(J+K) \sim \Delta \gg 1$ region, either the configuration $\{s_i = 0\}$ with all the spins zero, or the two configurations $\{s_i = s_j = \cdots = \pm 1\}$ with all the spins aligned completely dominate the ensemble. Their respective energies are

$$\mathcal{H}(\{s_i = 0\}) = 0 , \tag{2.3a}$$

$$\mathcal{H}(\{s_i = s_j = \cdots = \pm 1\}) = N[2(J+K) - \Delta] , \quad N \to \infty , \tag{2.3b}$$

where N, the number of lattice sites, it taken to infinity in the thermodynamic limit. Thus, at

$$2(J+K) = \Delta \gg 1 \tag{2.4}$$

domination abruptly passes from the zero configuration to the aligned configurations. This constitutes a first-order transition between a paramagnetic phase ($M = Q = 0$) at $2(J+K) < \Delta$ and two coexisting ferromagnetic phases ($M = \pm 1$, $Q = 1$) at $2(J+K) > \Delta$. The (three-phase coexistence) boundary (2.4) is represented in Fig. 1 by the plane F_3.

C. Griffiths symmetry

Griffiths[41] pointed out the following feature of the phase diagram: Consider the $J = 0$ plane. Since flipping any spin $s_i \to -s_i$ does not change

the energy of a configuration, the magnetization is zero. Define a new variable t_i at each site i by

$$t_i \equiv 2s_i^2 - 1 . \tag{2.5}$$

Substituting into (1.1), one obtains the equivalent problem

$$\mathcal{H}_t(J_t, H_t; \{t\}) = J_t \sum_{\langle ij \rangle} t_i t_j + H_t \sum_i t_i , \quad t_i = \pm 1 , \tag{2.6a}$$

where the new interaction constants are related to the original ones by

$$J_t = \tfrac{1}{4} K , \tag{2.6b}$$

$$H_t = K + \tfrac{1}{2}(\ln 2 - \Delta) . \tag{2.6c}$$

This is again the spin-$\frac{1}{2}$ Ising model (2.2), this time in a magnetic field H_t. All its phase transitions occur at $H_t = 0$, i.e., along the line $J = 0, \Delta = 2K + \ln 2$, labelled SF_2 in Fig. 1. The Onsager critical transition takes place at G:

$$J_G = 0, \quad K_G = 4J_{1/2}, \quad \Delta_G = 8J_{1/2} + \ln 2 . \tag{2.7}$$

Beyond ($K > K_G$) this point, GF_2 is a line of first-order transitions (two-phase coexistence) between two paramagnetic ($M \equiv \langle s_i \rangle = 0$) phases at $H_t \gtrless 0$ with $\langle t_i \rangle \gtrless 0$, i.e., $Q \gtrless \frac{1}{2}$.

This exact mapping between the $\Delta \ll -1$ region of Sec. II A and the $J = 0$, $\Delta = 2K + \ln 2$ line here constitutes a *symmetry* in the phase diagram.[42] This symmetry will be built into our PSRG transformation in Sec. III.

D. MFA phase diagram

To show how the above pieces can fit together, we now give the MFA phase diagram (Fig. 2) which later will be used for comparison with the PSRG phase diagram. In MFA each spin feels only the average presence of its neighbors, which amounts to ignoring fluctuations. The result can at best provide a qualitative indication of the true behavior of the model here. Several authors[28-31] have presented MFA phase diagrams for the BEG model. We have followed their approach to obtain the one in Fig. 2, in terms of the variables J, K, Δ which are appropriate for the renormalization-group calculation.

In this diagram, the two coexisting ferromagnetic ($M \gtrless 0$) phases and each of the two paramagnetic ($M = 0$, $Q \gtrless \frac{1}{2}$ in Para $_{\pm}$) phases are separated by the critical[40] transition surface CT_0E_3L, and by the first-order transition surfaces $F_3T_0E_3L$ (three-phase coexistence) and F_2GE_2L (two-phase coexistence). These surfaces are bounded by the ordinary tricritical[40,43] line T_0E_3, the isolated critical line GE_2, and the critical end line E_3L where critical and first-order transitions meet with no intervening higher-order transition. Similarly, E_2 and E_3 are, respectively, critical and tricritical end points. Between, E_2E_3 is a four-phase coexistence line. Representative constant-K cross sections are in Fig. 3. The conditions derived in Secs. II A–II C above and depicted in Fig. 1 are fulfilled by this MFA phase diagram. The PSRG phase diagram, Fig. 7, turns out to be qualitatively different in the E_2E_3 region.

III. RENORMALIZATION-GROUP TRANSFORMATION

A. General considerations

A position-space renormalization-group (PSRG) transformation is effected[5] by (i) grouping neighboring lattice *sites* into *cells*; (ii) associating with each cell a new spin variable *(cell spin)* which reflects a collective property of the initial spins *(site spins)* inside the cell; (iii) summing in the position-space representation of the partition function over all degrees of freedom orthogonal to the cell-spins. In the last step, one usually[4] resorts to some truncating[25] approximation to control the arbitrarily distant-neighbor, many-site interactions otherwise generated. Thus, the site-spin problem is converted into a cell-spin problem. One insures that both problems have the same *structure* (lattice type, spin kinematics, Hamiltonian functional form). The length *scale*, of course, is increased due to the thinning out of degrees of freedom.[1] The cell-spin Hamiltonian differs from the site-spin one by the values of the various interaction constants, so that repeated application of this procedure corresponds to discrete jumps in Hamiltonian space, as in Fig. 6. For easy visualization, we follow the usage of referring to these jumps as "flows" or "trajectories." From their analysis all thermodynamic information on the initial system can be extracted.

This general prescription leaves considerable freedom, specifically in steps (i) and (ii) above. As pointed out by van Leeuwen,[24] symmetry considerations should guide the final choice of a PSRG transformation. We adopt his approach by incorporating into our transformation the following known symmetries of the problem:

(a) We have seen in Sec. II that the BEG model reduces to spin-$\frac{1}{2}$ Ising models in two distinct regions: $\Delta \ll -1$ or $J = 0$. This constitutes the *Griffiths symmetry*.[41] We insure that our transformation acts in identical manner on either of these spin-$\frac{1}{2}$ Ising models.

(b) As usual, our transformation does not discriminate between positive and negative spin directions. This results in the *up-down symmetry* of classical spin systems: Any feature at a given

point of interaction-constant space is duplicated at the point arrived at by changing the sign of all odd interactions, for example, $(J_t, H_t) \to (J_t, -H_t)$ in (2.6a), or $(J, K, \Delta, H, L) \to (J, K, \Delta, -H, -L)$ in (1.1) and (1.2).

We perform step (i) by grouping neighboring sites into the simplest square cells as shown in Fig. 4(a). Each cell is referred to by a primed index i', and each site by $i'a$, $a = 1, 2, 3, 4$ clockwise as in the figure. We fulfill the above requirements (a) and (b) in step (ii). This involves sharing the 3^4 site-spin configurations $\{s_{i'1}, s_{i'2}, s_{i'3}, s_{i'4}\}$ among the three cell-spin configurations $s'_{i'} = 0, \pm 1$. As our basic building block, we use an assignment scheme applicable to the spin-$\frac{1}{2}$ Ising problem.

B. Spin-$\frac{1}{2}$ problem: majority rule

At each site $i'a$ in the cell i', a site spin $t_{i'a} = \pm 1$ was introduced in (2.5). We now associate with the whole cell a cell spin $t'_{i'} = \pm 1$ which is determined collectively by the four site spins $t_{i'a}$ inside the cell. The Hamiltonian $\mathcal{H}'_{t'}$ coupling the cell spins $\{t'\}$ is obtained from a Hamiltonian $\mathcal{H}_t$ coupling the site-spins $\{t\}$ by summing[5] in the position-space representation of the partition function over all degrees of freedom orthogonal to the cell-spins $\{t'\}$:

$$e^{\mathcal{H}'t'} = \sum_{\{t\}\text{fixed}\,\{t'\}} e^{\mathcal{H}t} . \tag{3.1}$$

This transformation as usual conserves[1,5] the partition function:

$$Z = \sum_{\{t'\}} e^{\mathcal{H}'t'} = \sum_{\{t\}} e^{\mathcal{H}t} . \tag{3.2}$$

Equation (3.1) may be expressed equivalently using a projection matrix[6-8,11]:

$$e^{\mathcal{H}'t'} = \sum_{\{t\}} \left(\prod_{i'} M(t'_{i'}; t_{i'a}) \right) e^{\mathcal{H}t} , \tag{3.3}$$

where the sum over site-spin configurations $\{t\}$ is now free. The total projection matrix appears as an outer product of single-cell projection matrices, reflecting our earlier choice of having the site spins $t_{i'a}$ in each cell determine their own cell spin $t'_{i'}$ exclusively.

$$\sum_{t'} M(t'; t_a) = M(1; t_a) + M(-1; t_a) = 1 \tag{3.4}$$

is sufficient for the partition function conservation (3.2). The most general single-cell projection matrix obeying the symmetries of the square and the up-down symmetry (b) of Sec. III A is

$$M_{p,q}(t'; t_a) = \tfrac{1}{2}\{1 + t'[\, p(t_1 + t_2 + t_3 + t_4) + q(t_1 t_2 t_3 + t_1 t_2 t_4 + t_1 t_3 t_4 + t_2 t_3 t_4)]\} . \tag{3.5}$$

A physically appealing cell-spin assignment is

$$t'_{i'} = \operatorname{sgn}(t_{i'1} + t_{i'2} + t_{i'3} + t_{i'4}) ,$$

$$\operatorname{sgn}(x) \equiv \begin{cases} 1, & x > 0, \\ 0, & x = 0, \\ -1, & x < 0, \end{cases} , \tag{3.6}$$

with the simple added proviso[16] that $t'_{i'} = \pm 1$ equally share the site-spin configurations summing to zero. (3.1) in conjunction with (3.6) is the form originally introduced by Niemeijer and van Leeuwen[5] and extensively employed in subsequent works.[9,10,12,13,15,22,24] The single-cell projection matrix (3.5) corresponding to (3.6) has the parameter values $p = \frac{3}{8}$, $q = -\frac{1}{8}$, and may be compactly written

$$M_{3/8,-1/8}(t'; t_a) = \frac{1}{2}\left[1 + t' \operatorname{sgn}\left(\sum_a t_a\right)\right] \equiv M_0(t'; t_a) . \tag{3.7}$$

The right-hand identity defines a projection matrix $M_0(t'; t_a)$ which will be useful in what follows and

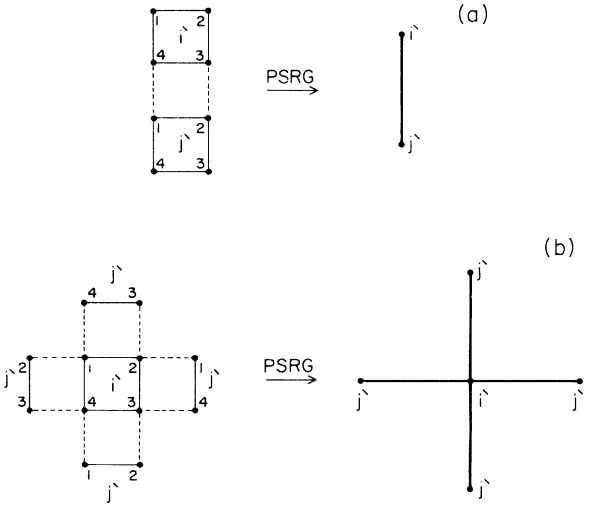

FIG. 4. Finite lattices for the derivation of truncated recursion relations. (a) The two-cell cluster as in Ref. 5; (b) the two-cell cluster with periodic boundary conditions. The latter corresponds to a checker-board pattern repetition of the two cells. It does not violate the position of the asymptotic first-order plane of Sec. II B and therefore is used in this work (see Sec. III D). Cells are referred to by the primed indices i', j', and sites by $i'a$, $j'a$, $a = 1, 2, 3, 4$ clockwise as shown. In this figure, intercell (intracell) site-spin interactions are shown with dashed (full) lines. The resulting cell-spin interactions are shown with darker lines.

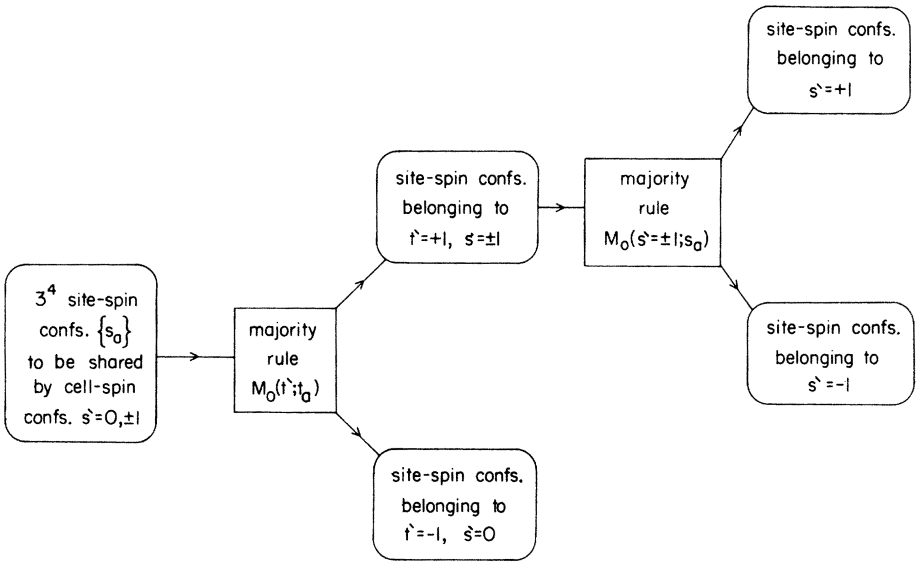

FIG. 5. Double majority rule described in Sec. III C. This procedure is condensed into the single-cell projection matrix of Eq. (3.9). It yields the PSRG transformation (3.8) containing the Griffiths and up-down symmetries of Sec. III A, and the symmetries of the square.

has a meaning independent[16] of the particular kinematics of the spins t_a. $M_0(t';t_a)$ embodies a cell-spin assignment which we shall refer to as *majority rule*.

C. Spin-1 problem: double majority rule

We are ready to proceed with the full kinematics of the BEG model: each site has a spin-1 variable $s_a = 0, \pm 1$, connected to the spin-$\frac{1}{2}$ variable of Sec. III B by $t_a \equiv 2s_a^2 - 1$; similarly each cell has a spin-1 variable $s' = 0, \pm 1$, connected to the spin-$\frac{1}{2}$ variable $t' \equiv 2s'^2 - 1$. Our object is to construct a single-cell projection matrix $P(s';s_a)$ for the spin-1 problem to be used in the transformation

$$e^{\mathcal{K}'s'} = \sum_{\{s\}} \left(\prod_{i'} P(s_{i'};s_{i'a}) \right) e^{\mathcal{K}s} . \tag{3.8}$$

The role of P is to allocate for each cell the 3^4 site-spin configurations $\{s_{a=1,2,3,4}\}$ among the three cell-spin values $s' = 0, \pm 1$. This is done in two stages (the following procedure is depicted in Fig. 5): First, we apply the majority rule $M_0(t';t_a)$ of (3.7). This splits the site-spin configurations into "magnetic" configurations ($s' = \pm 1, t' = 1$) and "nonmagnetic" configurations ($s' = 0, t' = -1$). Second, we subdivide the magnetic configurations into "up" configurations ($s' = 1$) and "down" configurations ($s' = -1$) by applying the majority rule $M_0(s' = \pm 1; s_a)$. The over-all effect is the single-cell projection matrix

$$P_0(s';s_a) = M_0(t';t_a)\left[(1 - s'^2) + s'^2 M_0(s';s_a)\right], \tag{3.9a}$$

or equivalently

$$P_0(s' = 0, \pm 1; s_a) = \begin{cases} M_0(t' = 1; t_a) M_0(s' = \pm 1; s_a) , \\ M_0(t' = -1; t_a) , \end{cases} \tag{3.9b}$$

the nonzero elements of which are collected in Table I.

The PSRG calculation performed with the *double majority rule* (3.9) is our main-line treatment. To distinguish it from a later variant we refer to it as PSRG ($v = 0$). PSRG ($v = 0$) contains the sym-

TABLE I. Nonzero elements of the spin-1 single-cell projection matrices. The values for negative cell-spin can be obtained from up-down symmetry: $P(s';s_a) = P(-s';-s_a)$. $v = 0$ gives the double majority rule of PSRG ($v = 0$); $v = -0.06453$ (see Ref. 45) gives the one-adjusted-parameter version PSRG ($v \neq 0$). Both transformations are described in Sec. III C.

$P(s' = +1, s_a)$	$P(s' = 0; s_a)$	$\{s_a\}$ any permutation of
1		+1, +1, +1, +1
$1 - v$		+1, +1, +1, −1
0.5		+1, +1, −1, −1
v		+1, −1, −1, −1
$1 - v$	v	+1, +1, +1, 0
$1 - v$	v	+1, +1, −1, 0
	v	+1, −1, −1, 0
	v	−1, −1, −1, 0
0.5	0.5	+1, +1, 0, 0
0.25	0.5	+1, −1, 0, 0
	0.5	−1, −1, 0, 0
v	$1 - v$	+1, 0, 0, 0
	$1 - v$	−1, 0, 0, 0
	1	0, 0, 0, 0

metries (a) (Griffiths) and (b) (up-down) of Sec. III A, and the symmetries of the square. It is physically motivated and has no adjustable parameters.[6,7,11] Its approximate (Sec. III D) treatment leads to our global phase diagram (Fig. 7) exactly reproducing the information of Secs. II A–II C and to transition temperatures and exponents with estimated inaccuracies of roughly 15% on the average.

In order to improve[44] the accuracy of our results, we have also employed a slightly modified version of our transformation: PSRG ($v\neq 0$) contains all the symmetries noted above, but also has a single adjustable parameter v [PSRG ($v\neq 0$) reduces to PSRG ($v=0$) when $v=0$]. We construct PSRG ($v\neq 0$) with a slight modification of the majority rule (3.7) applied to the spin-$\frac{1}{2}$ problem:

$$M_v(t';t_a)\equiv M_{S/8-v/2,v/2-1/8}(t';t_a)\,. \tag{3.10}$$

This projection matrix assigns the unanimous (i.e., $\{t_a\}=\{1,1,1,1\}$ and $\{-1,-1,-1,-1\}$ and evenly divided ($\{1,1,-1,-1\}$ and permutations) site-spin configurations as previously; however, an amount v of $\{1,1,1,-1\}$ is now assigned to $t'=-1$:

$$M_v(1;\{1,1,1,-1\})=1-v=M_v(-1;\{-1,-1,-1,1\})\,,$$
$$M_v(-1;\{1,1,1,-1\})=v=M_v(1;\{-1,-1,-1,1\})\,, \tag{3.11}$$

and similarly for any permutation of the site-spin values. The spin-1 single-cell projection matrix $P_v(s';s_a)$ used in PSRG ($v\neq 0$) is obtained by replacing M_0 by M_v for all the purely spin-$\frac{1}{2}$ factors (those with all site variables ± 1) in the right-hand side of (3.9b). Equivalently,

$$P_v(s';s_a)=M_v(t';t_a)\{(1-s'^2)+s'^2[(1-s_1^2s_2^2s_3^2s_4^2)M_0(s';s_a)+s_1^2s_2^2s_3^2s_4^2M_v(s';s_a)]\}\,, \tag{3.12}$$

the nonzero elements of which are in Table I. The parameter v is then adjusted[11] until at[45] $v=-0.06453$ it yields the correct[26] Onsager critical interaction (see Secs. II A and II C): $J_{1/2}=\frac{1}{2}\ln(1+\sqrt{2})$. We shall see in Secs. IV and V that this modest adjustment improves our quantitative results up to accuracies of a fraction of a percent!

D. Truncating approximation

The approach developed thus far cannot be carried out exactly. Starting, for example, with nearest-neighbor pair interactions only, such exact PSRG treatment generates[4] arbitrarily distant-neighbor, many-site interactions. For practical calculations one has to resort to some truncating[25] approximation.

We adapt Niemeijer and van Leeuwen's[5] two-cell cluster approximation: The recursion relations, which give the cell-spin interactions as functions of the site-spin interactions, are obtained by carrying out the PSRG transformation (3.8) on a finite lattice, viz., the two cells i' and j' shown in Fig. 4(a). However, note that the number of nearest-neighbor bonds per site is 1.25 for the finite lattice in Fig. 4(a), whereas it is 2 for infinite square lattice. This number directly affects the energy per site (2.3b) of the completely aligned spin configurations, and consequently the location (2.4) of the asymptotic first-order plane. Therefore, to get correct strong-coupling behavior we have used the periodic continuation of the two-cell cluster: the recursion relations are obtained from the finite lattice shown in Fig. 4(b). Specification of this cluster and the cell-site projection P [(3.9) or (3.12)] makes concrete the transformation (3.8). Because of the two-cell nature of our truncation, interactions remain nearest-neighbor pair or single spin. Furthermore, since we have built in up-down symmetry, the odd interactions H, L of (1.2) are not generated by the PSRG transformation unless they are initially present, i.e., the even subspace J, K, Δ of (1.1) is invariant. Examples of PSRG flows in this subspace are in Fig. 6.

E. Renormalization-group analysis

As mentioned earlier, the renormalization-group phase diagram is derived from the global

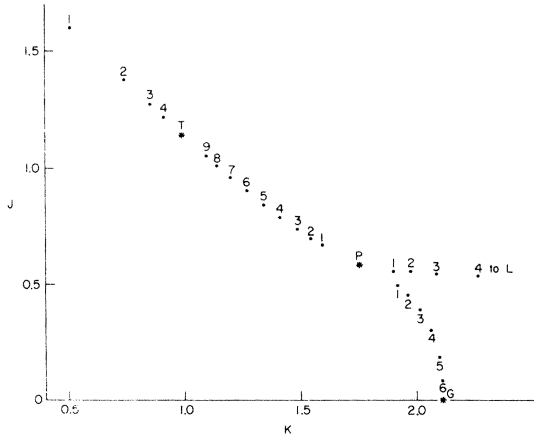

FIG. 6. Examples of renormalization-group flows, obtained in PSRG ($v=0$) (Sec. III D). The crystal-field interaction Δ is not shown. Consecutive jumps along each flow are indicated with numbers. Stars represent the fixed points G^*, T^*, P^* which are discussed in Secs. IV and V C. The closer the starting Hamiltonian is to a fixed point, the shorter is the jump: in principle, it takes infinitely many jumps to reach or leave a fixed point.

study of flows in Hamiltonian space, which are governed by *fixed points* (points invariant under the transformation). At such a fixed point, the correlation length ξ of the system is either zero or infinite.[1] In the latter case only, the entire *domain* of attraction (the subspace which eventually flows into the fixed point in question) shares the $\xi=\infty$ property. The two cases usually are distinguished quite easily by examination of the fixed-point Hamiltonian. For example, $\xi=0$ is ruled out when the fixed-point Hamiltonian contains finite couplings. Accordingly, fixed points and their domains can be classified as follows: (a) Higher-order fixed point ($\xi^*=\infty$, where the asterisk denotes fixed point): the domain is the locus of higher-order phase transitions. (b) First-order fixed point ($\xi^*=0$): the domain is the locus of first-order phase transitions. (c) Trivial fixed point ($\xi^*=0$): the domain is either (i) an entire thermodynamic phase, or (ii) the smooth continuation of one thermodynamic phase into another. We call these "phase sinks" or "continuation fixed points," respectively.[46] We shall have the opportunity of illustrating each of these types.

Critical (higher-order) exponents are obtained[1] by linearizing the recursion relations at the higher-order fixed point whose domain is the locus of the transitions in question. In our case, the recursion relations

$$[J',K',\Delta']=\mathfrak{F}[J,K,\Delta] \tag{3.13}$$

yield

$$J'-J^*=T_{JJ}(J-J^*)+T_{JK}(K-K^*)+T_{J\Delta}(\Delta-\Delta^*), \tag{3.14}$$

etc., where T_{JK} is the derivative $\partial J'/\partial K$ evaluated at the fixed point. The eigenvalues λ_l of this recursion matrix T_{XY} are written

$$\lambda_l=b^{y_l},\quad l=2,4,6, \tag{3.15}$$

where the length rescaling factor b is 2 in our case. A similar, independent linearization at the fixed point is performed by considering small deviations of the odd interactions H,L from their zero value, resulting in y_1,y_3. Unlike the eigenvalues λ_l, the "eigenvalue exponents" y_l are in principle transformation independent,[44] but not so in truncated calculations. We shall refer to the y_l simply as eigenvalues. The relevant eigenvalues $y_l>0$ give[1,5] higher-order (critical and tricritical) exponents from simple relations as seen in Secs. IV and V. Renormalization-group trajectories flow away from the fixed point along the eigendirections associated with these relevant y_l. The irrelevant eigenvalues $y_l<0$ give correction-to-scaling exponents.[47] Trajectories flow into the fixed point (from its domain) along the associated eigendirections.

IV. RESULTS

This section contains most of our results. We delay until Sec. V a unified presentation of PSRG-versus-MFA results for the three-state Potts model to which the BEG model reduces for specific values of the interaction-constant ratios. We shall be referring in general to results from the double majority rule PSRG ($v=0$) (Sec. III C). Those from the one-adjusted-parameter version PSRG ($v\neq0$) will be noted explicitly.

A. Over-all description

The BEG phase diagram, as obtained in the position-space renormalization-group treatment, is presented[48] in Fig. 7. The volume of the two quad-

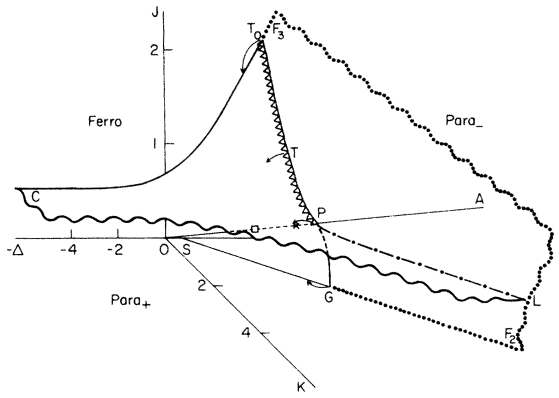

FIG. 7. BEG phase diagram (discussed in Sec. IV A) obtained in the position-space renormalization-group treatment PSRG ($v=0$). Critical and first-order transitions are, respectively, drawn with dark full and dotted lines. Wavy lines denote smooth continuation of surfaces. The two coexisting ferromagnetic phases (Ferro) and each of the two paramagnetic phases (Para$_\pm$) are separated by the critical surface CT_0PL, and by the first-order surfaces F_3T_0PL (three-phase coexistence) and F_2GPL (two-phase coexistence). T_0P is an ordinary tricritical line (triangles), GP is an isolated critical line, and PL is a critical end line (dash-dotted). P is a special tricritical point corresponding to the three-state Potts transition. On the Potts axis $0A$ (Secs. V B and V C), the cross marks the exact location of this transition, and the square marks the location of the first-order transition predicted by MFA. G,P,T are also the locations of the respective fixed points shown in Fig. 9; T_0 is the intersection of the tricritical line with the $K=0$ (Blume-Capel) plane. In the PSRG ($v\neq0$) version of our transformation, one parameter is adjusted so that the Griffiths-Onsager critical point G moves to its exact location. Some consequent changes are indicated with arrows. Representative constant-K cross sections of this PSRG phase diagram are in Fig. 8.

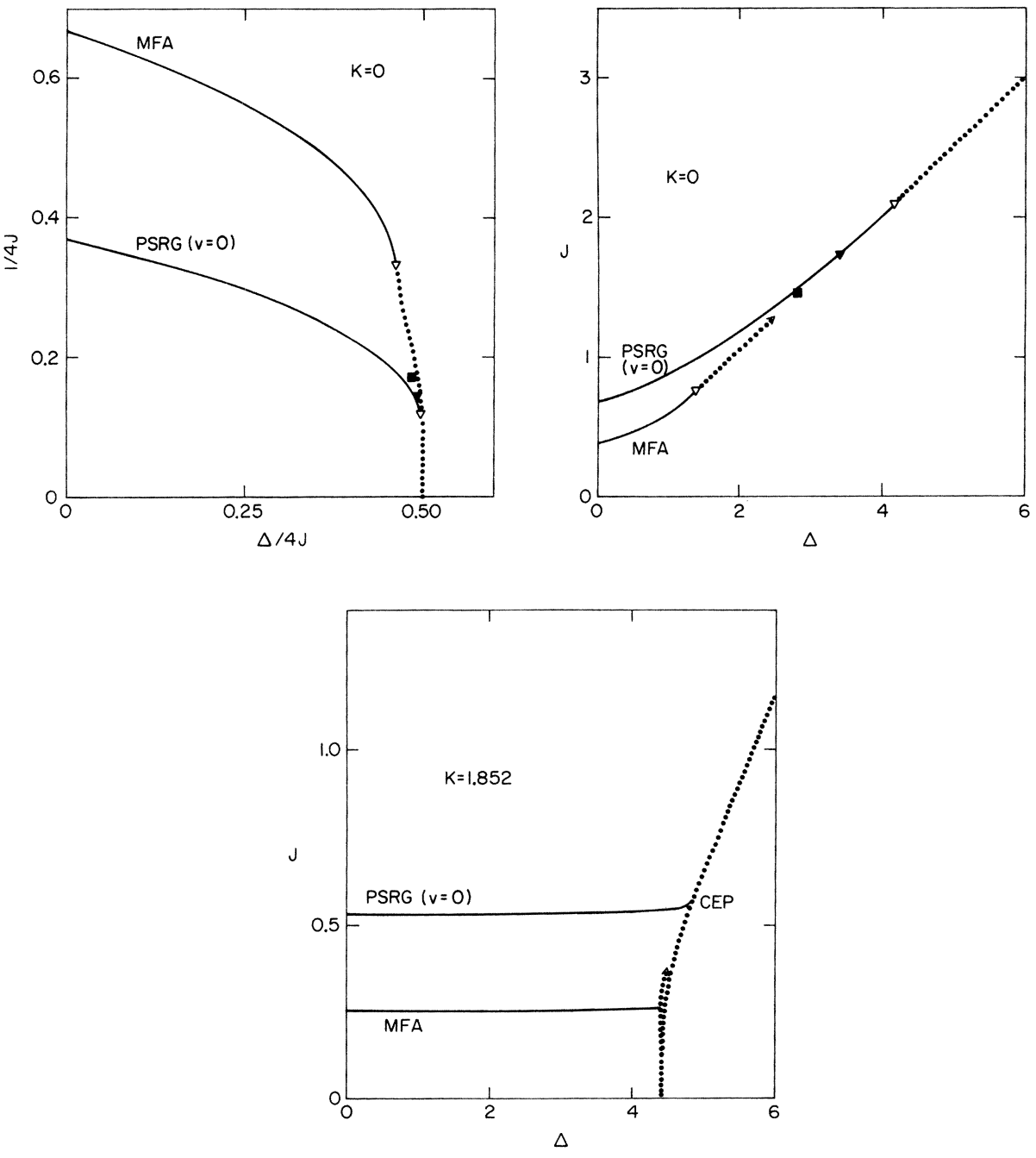

FIG. 8. Representative constant-K cross sections of the BEG phase diagram (Fig. 7) obtained in the position-space renormalization-group treatment PSRG ($v = 0$). (Portions of the corresponding MFA curves are also shown; an arrowhead denotes smooth continuation of curve). Critical and first-order transitions are, respectively, drawn with full and dotted lines. The Blume-Capel tricritical point (▽) and the critical end point (CEP) are indicated. The critical and first-order lines meet at the tricritical point with equal slopes. The two first-order lines at the critical end point have equal slopes, different from the slope of the critical line. The location of the tricritical point in our one-adjusted-parameter version PSRG ($v \neq 0$) is marked with ▼. In this figure, it is indistinguishable from that reported in Ref. 23. Its Monte Carlo location (Ref. 34) is marked with ■.

rants ($J, K \geq 0$) under study is divided by transition surfaces into three regions. Two of these are occupied by paramagnetic ($M \equiv \langle s_i \rangle = 0$) phases: One (labelled Para_+) has large quadrupole order parameter $Q \equiv \langle s_i^2 \rangle$, the other ($\text{Para}_-$) has small Q. In the remaining volume (Ferro), two ferromagnetic ($M \gtrless 0$) phases coexist. Thus, this whole region is actually a locus of first-order transitions between up and down magnetizations. These transitions would be manifest and the two ferromagnetic phases would be separated if an odd direction such as the magnetic field H were added to the phase diagram. The two paramagnetic phases $\text{Para}_\pm$ are separated by the first-order transition surface F_2GPL (two-phase coexistence), but merge at the isolated critical[40] line GP. Para_- and Ferro are separated by the first-order transition surface F_3T_0PL (three-phase coexistence). Para_+ and Ferro are separated by the critical transition surface CT_0PL. T_0P is a line of ordinary tricritical[40,43] points. PL is a line of critical end points (critical end line) where critical and first-order transitions meet with no intervening higher-order transition. The three lines GP, T_0P, and PL join at the special tricritical point P, corresponding to the transition of the three-state Potts model. The vicinity of P differs qualitatively from the E_2E_3 four-phase coexistence found in MFA (Fig. 2). This feature is discussed in Sec. V. The conditions derived in Secs. II A–II C and depicted in Fig. 1 are fulfilled by this PSRG ($v = 0$) phase diagram. Representative constant-K cross sections are in Fig. 8.

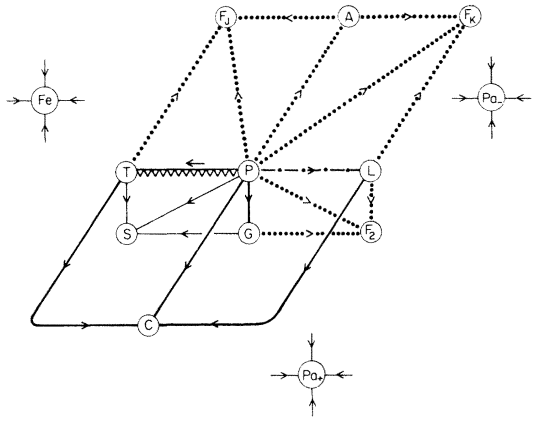

FIG. 9. Global connectivity of the 13 fixed points underlying the phase diagram in Fig. 7. Renormalization-group trajectories flowing through critical and first-order phase transitions are, respectively, drawn with dark full and dotted lines. The triangled and dash-dotted trajectories flow through the ordinary tricritical line and the critical end line, respectively. Light trajectories do not coincide with any phase transition. The classification and locations of these fixed points are given in Table II.

Thirteen fixed points underlie the phase diagram in Fig. 7. Their global connectivity is shown in Fig. 9. Their classification and locations are given in Table II. Linearization at fixed points with infinite interaction is done through appropriate changes of variable,[4] for example, e^{Δ} instead of Δ at C^*. Critical and first-order transitions and critical end-line behavior are discussed in Sec. IV B below. The ordinary tricritical properties are in Sec. IV C.

B. Critical and first-order transitions, critical end-line behavior

The fixed points C^* and G^*, respectively, provide the critical surface CT_0PL and the isolated critical line GP. As seen in Table II, C^* occurs in the $\Delta \ll -1$ region of Sec. II A, and G^* occurs in the $J = 0$ region of Sec. II C. Therefore, their locations are connected by the Griffiths symmetry (2.7):

$$K_G^* = 4J_C^*, \quad \Delta_G^* = 8J_C^* + \ln 2 . \tag{4.1}$$

The transition interaction $J_{1/2}$ of Secs. II A and II C is equivalent to J_C^* here, and turns out to be 0.5275 in PSRG ($v = 0$), 20% larger than the exact[26] value $\frac{1}{2}\ln(1+\sqrt{2}) \simeq 0.4407$. The parameter v in PSRG ($v \neq 0$) is adjusted so that this Onsager transition occurs at the exact value.[45] Then G^* moves to its exact location $(0, 2\ln(1+\sqrt{2}), 4\ln(1+\sqrt{2}) + \ln 2)$.

The eigenvalues of the two critical fixed points C^* and G^* are given in Table III. By Griffiths symmetry, $y_{2C} = y_{2G}$ and $y_{1C} = y_{4G}$. These, respectively, are the thermal and magnetic eigenvalues of the Onsager critical transition, and their exact values[26] are also given. The thermal eigenvalue is off by -27% in PSRG ($v = 0$), -6% in PSRG ($v \neq 0$). The magnetic eigenvalue is off by $+4\%$ in PSRG ($v = 0$), -0.3% in PSRG ($v \neq 0$). y_{3C} and y_{1G} are probably redundant eigenvalues,[49] which do not correspond to any new singularity or crossover in the free energy.[50]

Five fixed points in Table II provide the first-order transitions in our phase diagram. These fulfill the Nienhuis and Nauenberg conditions[51] for seeing first-order transitions in PSRG. Specifically, the largest eigenvalue y whose eigenfield couples to the discontinuous order parameter must equal the lattice dimensionality of the system ($d = 2$ in our case). This is exactly fulfilled for the five fixed points in question: The largest odd-interaction eigenvalue is 2 for each of Fe^*, F_J^*, A^*, F_K^*, yielding a discontinuous magnetization M. The largest even-interaction eigenvalue is 2 for each of F_J^*, A^*, F_K^*, F_2^* (also for L^*, see below),

TABLE II. Classification and locations of the fixed points underlying the phase diagram in Fig. 7. In PSRG ($v \neq 0$) G^* moves to the exact location (0, 1.7627, 4.2186) of the Griffiths-Onsager critical point. Correspondingly, P^* moves to (0.5319, 1.4761, 4.0119), to be compared with the exact location (0.5025, 1.5076, 4.0202) of the three-state Potts transition.

Fixed point	Type	PSRG ($v=0$) location (J^*, K^*, Δ^*)	Domain in J, K, Δ space (see Fig. 7)
	1. Higher-order fixed points		
C^*	Critical	$(0.5275, -0.1618, -\infty)$	Surface CT_0PL
G^*	Critical	(0, 2.1100, 4.9132)	Line GP
L^*	Critical end	$(0.5275, \infty, 2K^* + 1.0778)$	Line PL
T^*	Ordinary tricritical	(1.1390, 0.9944, 4.2449)	Line T_0P
P^*	Special tricritical (three-state Potts)	(0.5822, 1.7562, 4.6779)	Point P
	2. First-order fixed points		
Fe*	Discontinuous M	$(\infty, 0.4030 - J^*, -\infty)$ $J^*/\Delta^* = 0$	Volume Ferro
F_J^*	Discontinuous M, Q	$(\infty, \infty, 2(J^* + K^*))$ $3J^* - K^* = \infty$, $(3J^* - K^*)/\Delta^* = 0$	Portion of surface F_3T_0PL
A^*	Discontinuous M, Q	$(\infty, \infty, 2(J^* + K^*))$ $3J^* = K^*$	Line in surface F_3T_0PL
F_K^*	Discontinuous M, Q	$(\infty, \infty, 2(J^* + K^*))$ $K^* - 3J^* = \infty$, $(K^* - 3J^*)/\Delta^* = 0$	Remainder of surface F_3T_0PL
F_2^*	Discontinuous Q	$(0, \infty, 2K^* + \ln 2)$	Surface F_2GPL
	3. Trivial fixed points		
Pa_+^*	Sink for ($M=0$, large Q) phase	(0, 0, $-\infty$)	Volume Para_+
Pa_-^*	Sink for ($M=0$, small Q) phase	(0, 0, ∞)	Volume Para_-
S^*	Smooth continuation between preceding two phases	(0, 0, ln2)	Surface $SGPT_0$

TABLE III. Critical eigenvalues (Sec. IV B). $y_{2C} = y_{2G} = y_{2L}$ and $y_{4G} = y_{1C} = y_{1L}$ are the thermal and magnetic eigenvalues of the Onsager critical transition. The negative infinite eigenvalues y_{6C} and y_{6L} belong to deviations from $e^{\Delta_C^*} = 0$ and $e^{-K_L^*} = 0$; we found this typical of infinite interactions at fixed points. y_{1G}, y_{3C}, and y_{3L} are probably redundant eigenvalues (Refs. 49 and 50) which do not correspond to any new singularity or crossover in the free energy.

	PSRG ($v=0$)	G^* PSRG ($v \neq 0$)	Exact [a]	C^* PSRG ($v=0$)	Exact [a]	L^* PSRG ($v=0$)
y_2	0.7267	0.9419	1	0.7267	1	0.7267
y_4	1.9416	1.8697	1.875	−1.0492		2
y_6	−1.8338	−1.6375		$-\infty$		$-\infty$
y_1	0.5748	0.6628		1.9416	1.875	1.9416
y_3	−0.7327	−0.6731		0.3792		0.2355

[a] Reference 26.

yielding a discontinuous quadrupole order parameter Q. All other eigenvalues in our treatment are less than 2.

A schematic representation of the fixed-point structure yielding critical end-line behavior is in Fig. 10. The end-line fixed point L^* occurs[52] at $J_L^* = 0.5275$, $\Delta_L^* = 2K_L^* + 1.0778 = \infty$. The end line is in Fig. 7 the junction of the one critical and two first-order surfaces. L^* is correspondingly unstable (Fig. 10) towards C^* (critical), F_2^* (first-order in Q), and F_K^* (first-order in M and Q). The two-dimensional domains of these three fixed points meet along and are bounded by the one-dimensional (critical end) domain of L^*. The two first-order surfaces have equal slopes at the end line [Figs. 8(c) and 10]. As seen in Table III and Fig. 10, L^* has exactly the same relevant eigenvalues as C^*, namely the Onsager thermal and magnetic eigenvalues: $y_{2L} = y_{2C} = y_T$ and $y_{1L} = y_{1C} = y_h$. L^* also has another relevant even eigenvalue $y_{4L} = 2 = d$ characteristic of a first-order transition, which causes its additional instability. Thus in two distinct infinite interaction limits, $\Delta \ll -1$ and $\Delta \sim 2K \gg 1$, the recursion relations reduce in ways which yield the exact eigenvalue equality between the respective fixed points, and also the additional instability and first-order eigenvalue $y = d$ for L^*. This in general will be an appropriate mechanism for end-point behavior. In our case, y_T gives the critical singularity when L^* is approached along the dotted curve in Fig. 10, and $y_{4L} = 2 = d$ gives the first-order transition[51] in Q when L^* is approached along the full line. In summary, L^* appears as a hybrid of the one critical and two first-order fixed points it mediates.

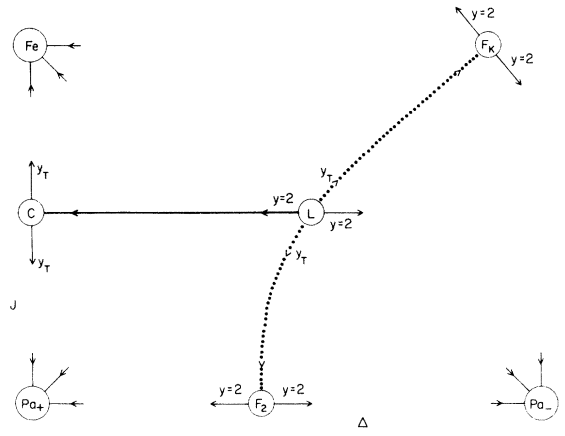

FIG. 10. Schematic representation of the fixed-point structure yielding critical end-line behavior, discussed in Sec. IV B. Critical and first-order boundaries are respectively drawn with dark full and dotted lines. y_T is the thermal eigenvalue of the Onsager transition. Each fixed point here is stable with respect to a third direction which, schematically, can be visualized as perpendicular to the figure. Thus, in J,K,Δ space, the two-dimensional (critical) domain of C^* is bounded by the one-dimensional (critical end) domain of L^*.

C. Ordinary tricritical properties

As seen in Figs. 7 and 8(b), the critical surface CT_0P and the (three-phase coexistence) first-order surface F_3T_0P are separated, without discontinuity in slope, by the line T_0P of tricritical[40,43] transitions. To distinguish from the "special" tricritical Potts transition in Sec. V, these are referred to as "ordinary" tricritical transitions (ordinary omitted in remainder of section). The fixed-point structure yielding them is schematically represented in Fig. 11. Thus, in J,K,Δ space, the two-dimensional (critical and first-order) domains of C^* and F_J^* are separated by the one-dimensional (tricritical) domain of T^*.

The location of the $K = 0$ (Blume-Capel[28]) tricritical point T_0, and the tricritical eigenvalues are given in Table IV, along with data from other works.[22,23,34,53] There are no exact results for comparison; however, the close agreement of our PSRG ($v \neq 0$) [expected to be more quantitative than our PSRG ($v = 0$)] with Burkhardt's[23] entirely different[7] PSRG on the same system, is quite en-

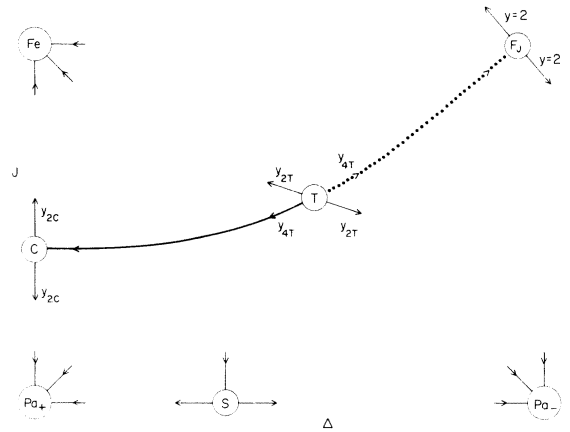

FIG. 11. Schematic representation of the fixed-point structure yielding ordinary tricritical behavior, discussed in Sec. IV C. Critical and first-order boundaries are, respectively, drawn with dark full and dotted lines. Each fixed point here is stable with respect to a third direction which, schematically, can be visualized as perpendicular to the figure. Thus, in J,K,Δ space, the two-dimensional (critical and first-order) domains of C^* and F_J^* are separated by the one-dimensional (tricritical) domain of T^*. The domain of the trivial fixed point S^* is a smooth continuation between the Para_+ and Para_- phases.

TABLE IV. Ordinary tricritical eigenvalues and the $K=0$ (Blume-Capel) tricritical point T_0 (Sec. IV C).

	PSRG ($v=0$)	PSRG ($v\neq 0$)	Other PSRG [a, b]		$\epsilon\equiv 3-d$ expansion, [c] Monte Carlo [d]
y_{2T}	1.9201	1.8373	1.7966 [a]	1.852 [b]	$2-\frac{4}{125}\epsilon^2=1.968$ [c]
y_{4T}	0.7192	0.9181	0.7983 [a]	0.652 [b]	$1+\frac{1}{5}\epsilon=1.2$ [c]
y_{6T}	−0.6654	−0.6875			$-2\epsilon=-2$ [c]
y_{1T}	1.9707	1.9296	1.9275 [a]		$\frac{5}{2}-\frac{1}{2}\epsilon-\frac{1}{1000}\epsilon^2=1.999$ [c]
y_{3T}	0.6785	0.8683	1.1063 [a]		$\frac{3}{2}+\frac{3}{10}\epsilon=1.8$ [c]
J_{T_0}	2.0960	1.7317	1.724 [a]		1.5 [d]
Δ_{T_0}	4.1689	3.4127	3.400 [a]		2.8 [d]

[a] Reference 23: PSRG on the same two-dimensional spin-1 Ising (BEG) model as in our work, but with a quite different truncating approximation.

[b] Reference 22: PSRG on the two-dimensional spin-$\frac{1}{2}$ Ising antiferromagnet, which by universality should have tricritical eigenvalues equal to the BEG model ones.

[c] Reference 53: momentum-space renormalization group on continuous, $n=1$ spin models, by expanding downwards from dimensionality three. Again, comparison is justified by universality.

[d] Reference 34: Monte Carlo study of the two-dimensional BEG model. J_{T_0} is deduced from their Fig. 1; then for Δ_{T_0}, their quoted $\Delta_{T_0}/4J_{T_0}=0.485$ [compare with 0.493 in our PSRG ($v\neq 0$)] is used.

couraging: The locations of T_0 differ only by 0.4%, y_{1T} and y_{2T} by +0.1% and +2%. We note that the latter two percentages parallel the accuracies of the two critical eigenvalues given in Sec. IV B. In general, magnetic eigenvalues seem most accurate. The smaller tricritical eigenvalues differ in the two works more: y_{4T} by +13%, y_{3T} by −27%. The slow convergence of nonleading eigenvalues has been observed previously.[5] We can also compare with Nienhuis and Nauenberg's[22] tricritical eigenvalues for the two-dimensional spin-$\frac{1}{2}$ Ising antiferromagnet, which by universality should equal those of the BEG model. Similar conclusions emerge. On the other hand, almost

TABLE V. Ordinary tricritical exponents (Sec. IV C).

		Exponents		
Singular behavior [a]	Relation to eigenvalues [b]	PSRG ($v\neq 0$)	Monte Carlo [c,d]	MFA
$M\sim\tau_2^{\beta_t}t$	$\beta_t=(d-y_{1T})/y_{2T}$	0.0383	0.09 ± 0.12 [c]	$\frac{1}{4}$
$\chi\equiv\frac{\partial M}{\partial H}\sim\tau_2^{-\gamma_t}t$	$\gamma_t=(2y_{1T}-d)/y_{2T}$	1.0119	1.0 ± 0.3 [c] 1.1 ± 0.4 [c]	1
$M\sim h_1^{1/\delta_t}t$	$\delta_t=y_{1T}/(d-y_{1T})$	27.40	10.8 ± 0.7 [c]	5
$Q_{\text{ferro}}-Q_{\text{para}}\sim\tau_4^{\omega_u}u$	$\omega_u=(d-y_{2T})/y_{4T}$	0.177	0.65 ± 0.10 [c] 0.58 ± 0.11 [d]	1
$Y\equiv\frac{\partial Q}{\partial\Delta}\sim\tau_2^{-\lambda_t}t$	$\lambda_t=(2y_{2T}-d)/y_{2T}$	0.911	0.53 ± 0.14 [d]	$\frac{1}{2}$

[a] The notation of Ref. 32 is used for exponents. τ_l (h_l) are small even (odd) interaction deviations from tricriticality: $\tau_2(h_1)$ along the strongest tricritical direction, τ_4 along the first-order phase boundary.

[b] $d=2$ is the lattice dimensionality.

[c] Reference 34: Monte Carlo study of the two-dimensional BEG model. Both the paramagnetic (lower entry) and ferromagnetic determinations of the susceptibility exponent γ_t are given. These are exactly equal in renormalization-group theory.

[d] Reference 35: Monte Carlo study of the two-dimensional spin-$\frac{1}{2}$ Ising antiferromagnet. Comparison is justified by universality.

all our tricritical exponents (Table V) deduced from these eigenvalues fall outside the error bars of Monte Carlo studies.[34,35] The Monte Carlo[34] tricritical point T_0 is also away from ours (Table IV). We have no insight into this discrepancy. Finally, the ϵ-expansion tricritical eigenvalues, obtained[53] from momentum-space renormalization group on continuous, $n=1$ spin models by expanding downwards from dimensionality three, are also given in Table IV. Again, little quantitative contact is established with our results.

V. THREE-STATE POTTS TRANSITION

A. Three-state Potts model as special case of BEG

The full BEG model Hamiltonian with both even (1.1) and odd (1.2) interactions reads

$$\mathcal{H}(J,K,\Delta,H,L;\{s\}) = J\sum_{\langle ij\rangle} s_i s_j + K\sum_{\langle ij\rangle} s_i^2 s_j^2 - \Delta\sum_i s_i^2 + H\sum_i s_i + L\sum_{\langle ij\rangle}(s_i s_j^2 + s_i^2 s_j), \quad s_i = 0, \pm 1. \tag{5.1}$$

We have mentioned in Sec. III A the up-down symmetry (built into our PSRG) of the corresponding partition function (2.1c): $Z(J,K,\Delta,H,L) = Z(J,K,\Delta,-H,-L)$, which follows from the change $s_i \rightarrow -s_i$ at every site, i.e., a relabeling of spin states which interchanges $-1 \rightarrow 1$. This in fact is part of a more general symmetry[29-31] following from a relabeling of spin states which arbitrarily permutes $s_i = 0, \pm 1$. We call this the three-state permutation symmetry. We complete its description by considering the interchange $0 \rightarrow 1$: Define a new spin u_i at each site as

$$u_i \equiv \begin{cases} 0, \\ 1, \\ -1, \end{cases} \quad \text{when} \quad s_i = \begin{cases} 1, \\ 0, \\ -1, \end{cases}, \tag{5.2a}$$

or equivalently

$$u_i \equiv 1 + \tfrac{1}{2} s_i - \tfrac{3}{2} s_i^2 . \tag{5.2b}$$

Substituting (5.2b) into (5.1), the following relation is easily derived:

$$Z(J,K,\Delta,H,L) = Z(\tilde{J},\tilde{K},\tilde{\Delta},\tilde{H},\tilde{L}), \tag{5.3a}$$

for

$$\tilde{J} = \tfrac{1}{4}(J + K - 2L), \tag{5.3b}$$

$$\tilde{K} = \tfrac{1}{4}(9J + K + 6L), \tag{5.3c}$$

$$\tilde{\Delta} = \tfrac{1}{2}(3zJ + zK - \Delta + 3H + 4zL), \tag{5.3d}$$

$$\tilde{H} = \tfrac{1}{2}(zJ - zK + \Delta + H), \tag{5.3e}$$

$$\tilde{L} = \tfrac{1}{4}(-3J + K + 2L), \tag{5.3f}$$

where z is the number of nearest neighbors of a site, e.g., four in our square lattice. This means any feature at a given point (J,K,Δ,H,L) of interaction-constant space is duplicated at $(\tilde{J},\tilde{K},\tilde{\Delta},\tilde{H},\tilde{L})$ as in (5.3b)–(5.3f).

What does the symmetry (5.3) imply for our present study? Almost all points with zero odd interactions map by (5.3b)–(5.3f) onto nonzero odd interactions, which is of no direct interest to our phase diagram in Fig. 7. The only exception is the line $0A$ in Figs. 2 and 7:

$$K = 3J, \quad \Delta = 2zJ = 8J, \quad H = L = 0, \tag{5.4}$$

where each point maps onto itself. It can be argued[54] from three-state permutation symmetry that, if there is a higher-order transition on this line, then each odd eigenvalue y_{2n+1} should also occur as an even eigenvalue. This eigenvalue degeneracy is of immediate concern to our study (see Sec. V C).

Furthermore, substitution of (5.4) into (5.1) reveals that on the line (5.4) the BEG Hamiltonian reduces to

$$\mathcal{H} = R\sum_{\langle ij\rangle}(\delta_{s_i s_j} - 1), \tag{5.5a}$$

where $\delta_{s_i s_j}$ is the Kronecker δ, and for $J \geq 0$

$$R = \sqrt{\tfrac{2}{37}}\,(J^2 + K^2 + \Delta^2)^{1/2} \tag{5.5b}$$

measures the distance along the line from the zero-interaction origin. This is the three-state Potts[18,19,36-39,56] model. It can also be visualized as composed of ferromagnetically coupled spins restricted to point into the $0°, \pm 120°$ directions of a plane. For a detailed description of three-state Potts phenomenology, the reader is referred to Straley and Fisher.[38] In the following Sec. V B, we see the MFA prediction for this model by analysis in Fig. 2. In Sec. V C, our PSRG results are presented. In both sections other works[19b,36,38,39,55,56] will be recalled.

B. MFA prediction

Let us scan along the Potts axis $0A$ in the MFA phase diagram of Fig. 2. 0 is the infinite-temperature (inverse temperature $\sim R = 0$) point and the Potts system is completely disordered. This disordered phase persists until the Potts axis intersects the four-phase coexistence line E_2E_3 at

$$R_{\mathrm{MFA}} = 4z^{-1}\ln 2 = \ln 2 . \tag{5.6}$$

At R_{MFA}, three ordered phases, each with net alignment in one of the three directions of the planar visualization mentioned above, come into coexistence with the disordered phase. Beyond

R_{MFA}, only the ordered phases coexist, while the Potts axis stays within the three-phase coexistence surface $F_3T_0E_3L$. Evidently R_{MFA} is a first-order transition point.

We now hasten to discredit this MFA prediction. Potts[36] proved by a dual transformation for the square lattice that, if (5.5) has a single phase transition, this is exactly located at

$$R_{\mathrm{exact}} = \ln(1+\sqrt{3}) \simeq 1.0051 , \tag{5.7}$$

so that R_{MFA} is -31% off. More seriously, Straley and Fisher[38] concluded from low-temperature series analysis that the transition is higher order, instead of first order. Noting the unusual geometries of the phase and composition diagrams,[38] they suggested that it is a special tricritical[40] point. Indeed, Baxter[39] showed that the square lattice, q-state Potts model is equivalent to a staggered ice-type (six-vertex) model, thereby deducing a first-order transition for $q>4$, but a higher-order transition for $q \leq 4$ covering our case.

C. PSRG results

The three-state Potts transition enters our PSRG treatment in the form of the completely unstable (Fig. 9 and Table VI) higher-order fixed point P^*. The ordinary tricritical line, the isolated critical line, and the critical end line join at P^* (Fig. 7). Thus, the four-phase coexistence line E_2E_3 in mean-field theory (Fig. 2) shrinks into a special tricritical point in renormalization-group theory. This is the realization within the two-dimensional BEG phase diagram of what other authors[38,39] have predicted within strictly Potts context.

Our PSRG transformation does not incorporate the complete three-state permutation symmetry (Sec. V A): although it contains the up-down symmetry following from $-1 \rightleftharpoons 1$ spin-state relabeling, it does not contain the symmetry (5.3) following from $0 \rightleftharpoons 1$ spin-state relabeling (5.2). In general, if one were capable of pursuing an exact calculation,[44] a renormalization-group transformation not containing a particular symmetry of the partition function would still yield such symmetry in the resulting physics. Our calculations are of course not exact, so we can anticipate deviations from the consequences (discussed in Sec. V A) of three-state permutation symmetry. However, we can benefit from this violation by using its magnitude as an indicator[8] of the extent of damage done by our truncation. The outcome is quite favorable, as seen below. Local PSRG treatments directly on Potts models, including their permutation symmetry, have been performed by Harris *et al.*[18] and Dasgupta.[19]

TABLE VI. Potts special tricritical eigenvalues (Sec. V C). See Eq. (5.8) for values of the Potts transition interaction.

	PSRG ($v=0$)	PSRG ($v \neq 0$)	Other PSRG [a]	$\epsilon \equiv d-1$ expansion [b]
y_{2P}	1.9416	1.8704	1.8715 [a]	$1+\epsilon=2$ [b]
y_{4P}	0.8327	1.1063	1.1806 [a]	$\epsilon=1$ [b]
y_{6P}	0.4645	0.5248	0.4570 [a]	
y_{1P}	1.9362	1.8692		
y_{3P}	0.3846	0.5304		

[a] Reference 19(b): PSRG directly on the two-dimensional three-state Potts model, with a truncating approximation quite different from ours.

[b] Reference 56: Migdal's method (Ref. 57) applied to Potts models.

The location of P^* (Table II) gives the Potts transition interaction $R_{0,v}$ as in (5.5):

$$\begin{aligned} R_0 &= 1.1696 \ \text{ in PSRG } (v=0) , \\ R_v &= 1.001\,535 \ \text{ in PSRG } (v \neq 0) , \end{aligned} \tag{5.8}$$

versus

$$R_{\mathrm{exact}} = 1.005\,053 .$$

Thus, while R_0 is $+16\%$ off from the exact value, R_v is only -0.3% off. Because of the symmetry violation of our approximate calculation, discussed above, P^* does not exactly occur on the Potts axis $0A$ (5.4): in PSRG ($v=0$), P^* is away from the axis by 6×10^{-4} of its distance from the zero-interaction origin 0; in PSRG ($v\neq0$), by 1.0%.

The eigenvalues of the Potts special tricritical point are given in Table VI. The eigendirection of y_{2P} is along the Δ axis by 99.97% in PSRG ($v=0$) and 99.6% in PSRG ($v\neq0$), so that it corresponds to an external field coupling to the order parameter Q. The eigendirection of y_{4P} is approximately along the Potts axis:

$$(v_J, v_K, v_\Delta) = \begin{cases} (0.13, 0.34, 0.93) & \text{in PSRG } (v=0) , \\ (0.15, 0.32, 0.93) & \text{in PSRG } (v \neq 0) , \end{cases} \tag{5.9}$$

compared to (0.12, 0.35, 0.93) for the Potts axis, so that it corresponds to the temperature of the Potts system. The eigendirection of y_{6P} corresponds to crossover to the tricritical fixed point T^* on one side, and crossover to the critical fixed points G^* and L^* on the other side. Again the close agreement of our PSRG ($v\neq0$) this time with Dasgupta's[19b] entirely different[7] PSRG directly on the Potts model, also in Table VI, is quite encouraging: y_{2P}, y_{4P}, y_{6P} differ by -6×10^{-4}, -7%, $+13\%$, respectively. Agreement gets better with higher eigenvalue, as with tricritical ones. The Potts exponents deduced from these eigenvalues are in reasonable agreement in Table VII with low-[38] and high-tem-

TABLE VII. Potts special tricritical exponents (Sec. V C).

Singular behavior [a]	Relation to eigenvalues [b]	Exponents PSRG ($v \neq 0$)	Series [c,d]
Specific heat $\sim \tau_4^{-\alpha_p}$	$\alpha_p = 2 - d/y_{4P}$	0.192	0.05 ± 0.10 [c]
$Q_{\text{aligned}} - Q_P \sim \tau_4^{\beta_p}$	$\beta_p = (d - y_{2P})/y_{4P}$	0.117	0.10 ± 0.01 [c]
$\frac{\partial Q}{\partial \Delta} \sim \tau_4^{-\gamma_p}$	$\gamma_p = (2y_{2P} - d)/y_{4P}$	1.574	1.5 ± 0.2 [c] 1.42 ± 0.05 [d]
$\frac{\partial^2 Q}{\partial \Delta^2} \sim \tau_4^{-(\gamma_p + \Delta_p)}$	$\Delta_p = y_{2P}/y_{4P}$	1.691	1.58 ± 0.15 [d]

[a] τ_4 is a small deviation along the eigendirection of y_{4P}, which corresponds to the temperature of the Potts system.
[b] $d = 2$ is the lattice dimensionality.
[c] Reference 38: low-temperature series analysis.
[d] Reference 55: high-temperature series analysis.

perature[55] series analysis. Each of the odd eigenvalues should by three-state permutation symmetry be degenerate[54] with an even eigenvalue. Indeed, y_{2P} and y_{1P}, y_{6P} and y_{3P} differ only by $+6 \times 10^{-4}$, -1% in PSRG ($v \neq 0$) [$+0.3\%$, $+17\%$ in PSRG ($v = 0$)].

Finally we point out that in both PSRG ($v = 0$) and PSRG ($v \neq 0$), the magnetic eigenvalue of the Onsager transition is numerically between the very close y_{1P} and y_{2P} (which should be equal by three-state permutation symmetry): In PSRG ($v \neq 0$), y_{2G} is only 2 parts in 10^4 more than y_{1P}, and 4 parts in 10^4 less than y_{2P}. On this basis we speculate that the magnetic eigenvalue $y_h = 1.875$ of the two-dimensional Ising critical transition is equal to its counterpart in the two-dimensional three-state Potts transition. This would imply the equality of the exponents determined solely by the magnetic eigenvalue: δ and η. An analogous situation occurs along a line of transitions in the eight-vertex ice-type model, where it is believed[58] the exponents involving the thermal eigenvalue continuously change from their Ising values, whereas δ and η remain fixed at their Ising values. (Baxter[39] showed that the square-lattice Potts model is equivalent to the six-vertex ice-type model.) Furthermore, Stephen[56] has recently performed an expansion in $\epsilon \equiv d - 1$ for the Ising-Potts models by using Migdal's method.[57] To first order in ϵ, he finds that both the magnetic and thermal eigenvalues in the two models are respectively equal. However, an approximate calculation[56] he does at $d = 2$ yields a thermal eigenvalue 11% larger for the three-state Potts model than for the Ising model, in agreement with our results.

ACKNOWLEDGMENTS

We are greatful to R. B. Griffiths for drawing our attention to the Potts transition and to C. Dasgupta for providing us with unpublished results. We thank M. Blume, J. Chalupa, M. E. Fisher, G. Grinstein, D. R. Nelson, and M. J. Stephen for helpful discussions. We acknowledge the hospitality of the Physics Department of the Brookhaven National Laboratory, where this research was initiated.

*Research supported in part by the National Science Foundation under Grants No. NSF DMR75-22241 and DMR72-03026.

[1] K. G. Wilson, Phys. Rev. B 4, 3174 (1971); B 4, 3184 (1971); K. G. Wilson and J. Kogut, Phys. Rep. 12 C, 75 (1974); M. E. Fisher, Rev. Mod. Phys. 46, 597 (1974).
[2] For general reviews, see M. E. Fisher, Rep. Prog. Phys. 30, 615 (1967); L. P. Kadanoff *et al.*, Rev. Mod. Phys. 39, 395 (1967); H. E. Stanley, *Introduction to Phase Transitions and Critical Phenomena* (Oxford U. P., Oxford, 1971).
[3] L. P. Kadanoff, Physics (N.Y.) 2, 263 (1966).
[4] For exact illustrations of position-space renormalization-group methods on one-dimensional models, see D. R. Nelson and M. E. Fisher, Ann. Phys. (N.Y.) 91, 226 (1975); S. Krinsky and D. Furman, Phys. Rev. Lett. 32, 731 (1974); Phys. Rev. B 11, 2602 (1975); M. Nauenberg, J. Math. Phys. 16, 703 (1975); G. Grinstein *et al.* in Ref. 20. Because of the limited lattice connectivity in these models, it is possible to avoid generating arbitrarily distant-neighbor, many-site interactions.

[5]Th. Niemeijer and J. M. J. van Leeuwen, Phys. Rev. Lett. 31, 1411 (1973); Physica (Utr.) 71, 17 (1974); in *Phase Transitions and Critical Phenomena*, edited by C. Domb and M. S. Green (Academic, New York, to be published), Vol. 6; J. M. J. van Leeuwen in *Fundamental Problems in Statistical Mechanics*, edited by E. G. D. Cohen (North-Holland, Amsterdam, 1975), Vol. 3.

[6]L. P. Kadanoff and A. Houghton, Phys. Rev. B 11, 377 (1975).

[7]L. P. Kadanoff, Phys. Rev. Lett. 34, 1005 (1975); L. P. Kadanoff, A. Houghton, and M. C. Yalabik, J. Stat. Phys. 14, 171 (1976).

[8]K. G. Wilson, Rev. Mod. Phys. 47, 773 (1975).

[9]M. Nauenberg and B. Nienhuis, Phys. Rev. Lett. 33, 944 (1974); 33, 1598 (1974); B. Nienhuis and M. Nauenberg, Phys. Rev. B 11, 4153 (1975).

[10]J. A. Tjon, Phys. Lett. A 49, 289 (1974).

[11]K. Subbarao, Phys. Rev. B 11, 1165 (1975); 13, 3939 (1976).

[12]S.-C. Hsu, Th. Niemeijer, and J. D. Gunton, Phys. Rev. B 11, 2699 (1975).

[13]Aa. S. Sudbø and P. C. Hemmer, Phys. Rev. B 13, 980 (1976).

[14]M. N. Barber, J. Phys. C 8, L203 (1975).

[15]J. N. Fields and M. B. Fogel, Physica (Utr.) A 80, 411 (1975).

[16]A "spin-restructuring" transformation was introduced in A. N. Berker, Phys. Rev. B 12, 2752 (1975) to obtain the critical temperatures of higher-spin Ising models.

[17]See D. M. Lublin, Phys. Rev. Lett. 34, 568 (1975) for a two-dimensional classical XY model calculation. See D. D. Betts and M. Plischke, Can. J. Phys. 54, 1553 (1976); J. Rogiers and R. Dekeyser, Phys. Rev. B 13, 4886 (1976), for the quantum-mechanical case.

[18]A Potts model calculation is done in A. B. Harris, T. C. Lubensky, W. K. Holcomb, and C. Dasgupta, Phys. Rev. Lett. 35, 327 (1975).

[19]Potts model calculations are done in (a) C. Dasgupta, Phys. Rev. B 14, 1221 (1976); C. Dasgupta (unpublished).

[20]A. B. Harris and T. C. Lubensky, Phys. Rev. Lett. 33, 1540 (1974); A. P. Young and R. B. Stinchcombe, J. Phys. C 8, L535 (1975); T. Tatsumi and K. Kawasaki, Prog. Theor. Phys. 55, 612 (1976); K. Kawasaki and T. Tatsumi, *ibid.* 55, 614 (1976); G. Grinstein, A. N. Berker, J. Chalupa, and M. Wortis, Phys. Rev. Lett. 36, 1508 (1976).

[21]H. J. F. Knops, J. Phys. A 8, 1508 (1975), has obtained for a two-dimensional Ashkin-Teller model a phase diagram with three critical lines joining at one special point corresponding to the higher-order transition of the four-state Potts model.

[22]B. Nienhuis and M. Nauenberg, Phys. Rev. B 13, 2021 (1976), have obtained for a two-dimensional Ising antiferromagnet a phase diagram with critical and first-order surfaces separated by a tricritical line.

[23]Th. W. Burkhardt, Phys. Rev. B 14, 1196 (1976).

[24]J. M. J. van Leeuwen, Phys. Rev. Lett. 34, 1056 (1975).

[25]The term "truncating," due to M. E. Fisher, points to the fact that the approximation is uncontrolled, with no apparent small parameter. All justification is *a posteriori*, either through comparison with known information, or through convergence of a sequence of approximations. The latter is usually limited by calculational difficulties. Truncating approximations have been cluster calculations (finite-lattice recursion relations, Refs. 5, 8–11, 14, 18, 20, and 22, and this research), cumulant expansions (expansions in intercell interactions, Refs. 5, 6, 12, 13, 15–17, 20, and 21), and variational lattice decouplings by potential moving (Refs. 7, 19, and 23).

[26]L. Onsager, Phys. Rev. 65, 117 (1944); C. N. Yang, *ibid.* 85, 809 (1952).

[27]For previous work in this spirit, see Refs. 21 and 22.

[28]M. Blume, V. J. Emery, and R. B. Griffiths, Phys. Rev. A 4, 1071 (1971). Earlier works with no biquadratic exchange interaction ($K=0$) are M. Blume, Phys. Rev. 141, 517 (1966); H. W. Capel, Physica (Utr.) 32, 966 (1966); 33, 295 (1967); 37, 423 (1967).

[29]J. Lajzerowicz and J. Sivardière, Phys. Rev. A 11, 2079 (1975); J. Sivardière and J. Lajzerowicz, *ibid.* 11, 2090 (1975); 11, 2101 (1975).

[30]D. Mukamel and M. Blume, Phys. Rev. A 10, 610 (1974).

[31]D. Furman, S. Dattagupta, and R. B. Griffiths, Carnegie-Mellon University report (1976) (unpublished).

[32]D. M. Saul, M. Wortis, and D. Stauffer, Phys. Rev. B 9, 4964 (1974).

[33]A. K. Jain and D. P. Landau, Bull. Am. Phys. Soc. 21, 231 (1976).

[34]B. L. Arora and D. P. Landau, AIP Conf. Proc. 10, 870 (1973).

[35]D. P. Landau, Phys. Rev. Lett. 28, 449 (1972).

[36]R. B. Potts, Proc. Camb. Philos. Soc. 48, 106 (1952).

[37]For renormalization-group approaches to continuum-generalized Potts models, see G. Golner, Phys. Rev. B 8, 3419 (1973); R. G. Priest and T. C. Lubensky, *ibid.* 13, 4159 (1976).

[38]J. P. Straley and M. E. Fisher, J. Phys. A 6, 1310 (1973).

[39]R. J. Baxter, J. Phys. C 6, L445 (1973).

[40]We recall that at criticality (tricriticality) two (three) coexisting phases become indistinguishable.

[41]R. B. Griffiths, Physica (Utr.) 33, 689 (1967).

[42]Other phase-diagram symmetries are the up-down symmetry (Sec. III A) and the three-state permutation symmetry (Sec. V A).

[43]R. B. Griffiths, Phys. Rev. Lett. 24, 715 (1970).

[44]It should be noted that if one were capable of pursuing exact calculations, two distinct choices of renormalization-group transformations, such as PSRG ($v=0$) and PSRG ($v\neq 0$) here, would yield identical physics. This is simply because either procedure would amount to an exact, stepwise evaluation of the same initial partition function. However, the choice of transformation does affect results in truncated calculations. See, T. L. Bell and K. G. Wilson, Phys. Rev. B 10, 3935 (1974); 11, 3431 (1975); and Refs. 6, 7, and 11.

[45]The value $v=-0.064\,529\,434\,769\,360\,752$, which reproduces the Onsager critical temperature to 15 figures, was actually used.

[46]This distinction can depend on the interaction space considered. For example, a certain fixed point can have the role of phase sink in one interaction space, and that of continuation fixed point with the inclusion of more interaction types.

[47]F. J. Wegner, Phys. Rev. B 5, 4529 (1972).

[48]For phase-diagram data in tabular form, see A. N.

Berker, Ph.D. thesis (University of Illinois, 1977) (unpublished).

[49]F. J. Wegner, J. Phys. C 7, 2098 (1974); K. Subbarao, Phys. Rev. B (to be published).

[50]The likely mechanism is that they induce a "pseudocrossover" to another fixed point (at finite values of the odd interactions) which corresponds to the same type of phase transition as the original one. For examples of pseudocrossover, see D. R. Nelson and M. E. Fisher, Phys. Rev. B 11, 1030 (1975); Ref. 22 above.

[51]B. Nienhuis and M. Nauenberg, Phys. Rev. Lett. 35, 477 (1975).

[52]An argument similar to Sec. IIA justifies equal critical J values around L^* and C^*, a result also produced by MFA.

[53]M. J. Stephen and J. L. McCauley, Jr., Phys. Rev. Lett. A 44, 89 (1973); T. S. Chang, G. F. Tuthill, and H. E. Stanley, Phys. Rev. B 9, 4882 (1974); G. F. Tuthill, J. F. Nicoll, and H. E. Stanley, *ibid.* 11, 4579 (1975); F. J. Wegner, Phys. Lett. A 54, 1 (1975).

[54]The argument for the eigenvalue degeneracy of a Potts transition viewed in the spin-1 Ising interaction space goes as follows: Consider a higher-order phase transition on the Potts axis (5.4) and assume it is described by a renormalization-group treatment with built in three-state permutation symmetry. Then the corresponding fixed point $\vec{K}_P^*$ will occur in the interaction subspace in which each point maps onto itself under three-state permutation (Potts subspace). By up-down symmetry, the eigendirections at $\vec{K}_P^*$ can be constructed as purely even or odd. Consider a small deviation from $\vec{K}_P^*$ along any given odd eigendirection (therefore out of the Potts subspace) with eigenvalue y_{2n+1}. The $0 \longleftrightarrow 1$ spin state interchange (5.2) will map this "eigendeviation" onto another deviation with both even and odd components. Because of the built in three-state permutation symmetry of the renormalization group, the latter deviation will also be an eigendeviation, with the same eigenvalue y_{2n+1}. On the other hand, since the eigendirections can be constructed as purely even or odd, this implies the existence of an even eigendirection with eigenvalue equal to y_{2n+1}.

[55]D. Kim and R. I. Joseph, J. Phys. A 8, 891 (1975).

[56]M. J. Stephen, Harvard University report (1976) (unpublished).

[57]A. A. Migdal, Sov. Phys.-JETP (to be published).

[58]J. D. Gunton and Th. Niemeijer, Phys. Rev. B 11, 567 (1975).